Journal of Hazardous Materials 162 (2009) 212–221

Contents lists available at ScienceDirect

Journal of Hazardous Materials

journal homepage: www.elsevier.com/locate/jhazmat

Permeability optimization and performance evaluation of hot aerosol filters made using foam incorporated alumina suspension

Murilo D.M. Innocentini[a,*], Vanessa P. Rodrigues[a], Roberto C.O. Romano[b], Rafael G. Pileggi[b], Gracinda M.C. Silva[c], José R. Coury[c]

[a] Chemical Engineering Course, University of Ribeirão Preto, Av. Costábile Romano, 2201, Ribeirânia, 14565-380 Ribeirão Preto, SP, Brazil
[b] Civil Engineering Department, University of São Paulo, Av. Prof. Almeida Prado, travessa 2, no. 83, 05424-970 São Paulo, SP, Brazil
[c] Chemical Engineering Department, Federal University of São Carlos, Via Washington Luiz - km 235, 13565-905 São Carlos, SP, Brazil

ARTICLE INFO

Article history:
Received 29 December 2007
Received in revised form 4 May 2008
Accepted 6 May 2008
Available online 13 May 2008

Keywords:
Aerosol filtration
Hot gas filtration
Ceramic filters
Cellular ceramics
Permeability

ABSTRACT

Porous ceramic samples were prepared from aqueous foam incorporated alumina suspension for application as hot aerosol filtering membrane. The procedure for establishment of membrane features required to maintain a desired flow condition was theoretically described and experimental work was designed to prepare ceramic membranes to meet the predicted criteria. Two best membranes, thus prepared, were selected for permeability tests up to 700 °C and their total and fractional collection efficiencies were experimentally evaluated. Reasonably good performance was achieved at room temperature, while at 700 °C, increased permeability was obtained with significant reduction in collection efficiency, which was explained by a combination of thermal expansion of the structure and changes in the gas properties.

1. Introduction

The operation of the Brazilian sugarcane sector uses great amounts of thermal, mechanics and electric energies. Most of that energy is self-generated in the industry by the burnout of dry biomass residues (bagasse and straw) [1]. The rational use of those residues and the employment of the appropriate combustion technology would allow the production of spare electric power to be available in the market. It is estimated that additional energy could represent up to 10% of the installed potency of electricity generation in the country.

Hot gas cleaning technologies has played an increasingly important role in such cogeneration plants. The flue gases must be previously cleaned to avoid damage of downstream equipments or components and also to meet atmospheric emission regulations [1–3].

The ability to withstand high temperatures with very high efficiency has made ceramic filters useful to allow savings in thermal energy with simultaneous removal of particulate material and chemical contaminants from flue gases [4,5]. In order to be successfully employed, ceramic filters must have their permeability optimized, since one of the main drawbacks of this technology is the high pressure drop through the filtering elements.

The pressure drop is influenced not only by the operational conditions (gas velocity, temperature, etc.), but also by the permeability constants of the medium, which are features only of the porous structure. By carefully tailoring pore-related variables such as morphology, size and volume fraction, the optimization of permeability constants of ceramic filters can be achieved during the processing step [6–10]. However, careful attention must be given to interdependent variables such as mechanical strength and particle collection efficiency to ensure that they are compromised. This balance of variables is crucial for the development of an efficient, stable and durable hot gas filter system.

In this work, the procedure to evaluate the range of permeability constants required for a maximum acceptable pressure drop is discussed. The procedure is applied to optimize the permeability of filters prepared by the technique of incorporation of aqueous foams into alumina suspensions [6]. The selected bodies had their permeability and dust collection efficiency tested at room temperature and 700 °C.

1.1. Permeability optimization of ceramic membranes

Permeability is a macroscopic measure of the ease with which a fluid driven by a pressure gradient flows through the voids of a

* Corresponding author. Tel.: +55 16 3603 6784; fax: +55 16 3603 6718.
E-mail address: muriloinnocentini@yahoo.com.br (M.D.M. Innocentini).

0304-3894/$ – see front matter © 2008 Elsevier B.V. All rights reserved.
doi:10.1016/j.jhazmat.2008.05.025

porous medium. A suitable description of permeability for a given application must therefore combine aspects of fluid, porous structure and flow [11].

Forchheimer's equation is an example of a relationship well accepted in the literature that expresses the parabolic relationship between the pressure drop (ΔP) through the medium and the resulting superficial velocity (v_s) [11–16]:

$$\frac{\Delta P}{L} = \frac{\mu v_s}{k_1} + \frac{\rho v_s^2}{k_2} \quad (1)$$

For incompressible flow (liquids):

$$\Delta P = P_i - P_o \quad (2)$$

and for compressible flow (gases and vapours):

$$\Delta P = \frac{P_i^2 - P_o^2}{2P} \quad (3)$$

in which P_i and P_o are, respectively, the absolute fluid pressures at the entrance and exit of the membrane, μ and ρ are, respectively, the fluid viscosity and density. P is the pressure (either P_i or P_o) for which v_s, μ and ρ are measured or calculated.

For hot aerosol filtration conditions, the pressure drop through the membrane is small compared with the system pressure and the error associated with the use of Eq. (2) is usually smaller than 2%.

For rigid porous ceramics, the contribution of the structure in Eq. (1) is quantified by the thickness L and permeability parameters k_1 and k_2, which are complex functions of the morphology, size distribution, connectivity and volume of the void fraction [11]. Usually, these parameters are referred to as permeability constants, since they are supposed to be independent of both fluid and flow conditions, even though they may vary with temperature. The terms k_1 and k_2 are thus known as *Darcian* and *non-Darcian* permeability constants, in reference to Darcy's law, a simpler and earlier empirical model for permeability description [11,17].

Eq. (1) helps to quantify how much energy (pressure) is necessary to force the gas to percolate the filtering membrane with a required velocity v_s.

The major costs involving hot aerosol filtration processes are related to the filtration area (expressed by the number of filtering elements), to the pressure drop (expressed by the electric power of the fan) and to the membrane lifetime (expressed by the frequency of elements replacement).

The power consumption W is directly proportional to the pressure drop ΔP and to the volumetric flow rate Q:

$$W = \frac{Q\,\Delta P}{\eta} \quad (4)$$

in which η is the fan efficiency (usually between 0.55 and 0.80).

Typically, Q is specified from the application and the filtration area A is calculated from $A = Q/v_s$ to give an acceptable pressure drop or a power consumption W. Then the number of filtering elements n is obtained from the area A_i of each element ($n = A/A_i$). From the industrial standpoint, hot aerosol filtration operates in gas velocities around 0.01–0.1 m/s, with acceptable pressure drop for the virgin medium lower than 1000 Pa (≈10 cmH_2O) [5,12,18,19]. Higher velocity values are desirable, but they may cause increase of pressure drop to unfeasible levels and the penetration of fine particles, with progressive clogging of the void fraction and decrease of the filter lifetime.

The alternatives to minimize costs due to power and area constraints are the reduction of membrane thickness L or the increase of permeability constants k_1 and k_2. The former option can be achieved during the membrane processing, promotes linear savings in power costs and does not affect collection efficiency, but it may endanger the membrane mechanical strength and thus its lifetime.

Reduction in pressure drop can also be achieved by increases in k_1 and k_2, and the intensity of this reduction will depend on the weight of each term on the right side of Forchheimer's equation. The linear term $[\mu v_s/k_1]$ represents viscous energy losses due to friction between fluid layers. On the other hand, the quadratic term $[\rho v_s^2/k_2]$ represents the kinetic energy losses due to changes in the direction of motion and to acceleration or deceleration of the fluid caused by changes in the flow path (contraction or enlargement of the pore section or pore tortuosity along the flow direction). As stated by Hlushkou and Tallarek [17], viscous forces assist in the equalization of velocities at neighbouring points, i.e., in smoothing out small-scale heterogeneities in the flow. By contrast, inertial forces producing mixing of different fluid volumes result in a transfer of energy from large-to-small-scale components and, as a consequence, assist in the formation in the flow of heterogeneities characterizing turbulent flow.

It is worth noting that both viscous and inertial effects occur within the laminar flow regime, for which the pore Reynolds number ($Re_{pore} = \rho v_s d_{pore}/\varepsilon\mu$) is lower than 1 for predominance of viscous effects (Darcy's law) and $1 < Re_{pore} < 150$ for predominance of inertial effects. The onset of turbulence in a porous medium is in fact identified with $Re_{pore} > 300$ [17].

In order to make the macroscopic analysis easier, Eq. (1) can be rewritten in terms of Forchheimer's number (Fo) as [11]:

$$\frac{\Delta P}{L} = \frac{\mu v_s(1 + Fo)}{k_1} \quad (5)$$

$$Fo = \frac{v_s(k_1/k_2)}{\nu} \quad (6)$$

in which ν is the kinematic viscosity of the fluid ($\nu = \mu/\rho$).

The Fo parameter represents the ratio between kinetic and viscous forces that contribute for fluid pressure drop. Since the ratio k_1/k_2 is expressed as length, Forchheimer number can be understood as an analogous of the pore Reynolds number Re_{pore}. Fo is related to the linearity in the pressure drop curve in the same way that Re_{pore} is related to the laminarity of flow [11].

In order to minimize the inertial effects on the pressure drop, the Fo parameter must be small ($Fo \ll 1$), when Equation (5) is simplified to Darcy's law. Once ρ and μ are fixed from the process (temperature and pressure of gas stream), then Fo reduction is achieved by the decrease of the ratio k_1/k_2 or by the reduction of the face velocity v_s. This latter case must be disregarded, as it implies lower filtration rates. Thus, the requirement is the optimization of the ratio k_1/k_2 through changes in the structural features of the filtering element.

Data gathered from the literature show that k_1 and k_2 constants do not change independently of each other during processing, but are fairly linked instead through a single trend, regardless the type of porous structure (granular, fibrous or cellular) [11]. Although no satisfactory explanation for this trend has been given so far, it is useful for design purposes when no experimental k_2 data is available. Thus:

$$k_2 = \exp\left(\frac{-1.71588}{k_1^{0.08093}}\right) \quad (7)$$

Substitution of Eq. (7) in (1) then gives:

$$\frac{\Delta P}{L} = \frac{\mu v_s}{k_1} + \frac{\rho {v_s}^2}{\exp(-1.71588/k_1^{0.08093})} \quad (8)$$

The set of Eqs. (1)–(8) can be used to establish the requirements for permeability constants k_1 and k_2 in order to minimize ΔP for a chosen filtration velocity v_s or to maximize v_s for a chosen ΔP.

The following procedure can be used for flat membranes (disks or panels):

(1) assessment of operational gas flow conditions: temperature T, pressure P and volumetric flow rate Q;
(2) estimation of fluid properties μ and ρ for the operational conditions;
(3) selection of a target pressure drop ΔP for the process (usually, $\Delta P < 1000$ Pa);
(4) selection of a target superficial velocity v_s for the process (usually, $0.10\ \text{m/s} > v_s > 0.01\ \text{m/s}$);
(5) selection of a target thickness L for the filter element (usually, $L < 0.03$ m);
(6) use of Eq. (8) to find required constant k_1;
(7) use of Eq. (7) to find required constant k_2;
(8) verification of the weight of linear and parabolic terms of Forchheimer's equation through Fo in Eq. (6);
(9) use of k_1, k_2, L, ρ and μ values in Eq. (1) to simulate other flow conditions ($\Delta P \times v_s$) of interest;
(10) calculation of required filtration area A ($A = Q/v_s$);
(11) calculation of number of filtering elements based on the single unit area ($n = A/A_i$).

As an example of such procedure, Fig. 1a and b shows the necessary range of k_1 and k_2 values for flat clean ceramic elements of different thicknesses to result in a pressure drop of 1000 Pa during airflow at ambient conditions (25 °C and 760 mmHg). It is observed from Fig. 1c that pressure drop will display a fairly linear dependence with velocity ($Fo \ll 1$). Therefore, although both k_1 and k_2 values should be available for analysis, in this flow condition only

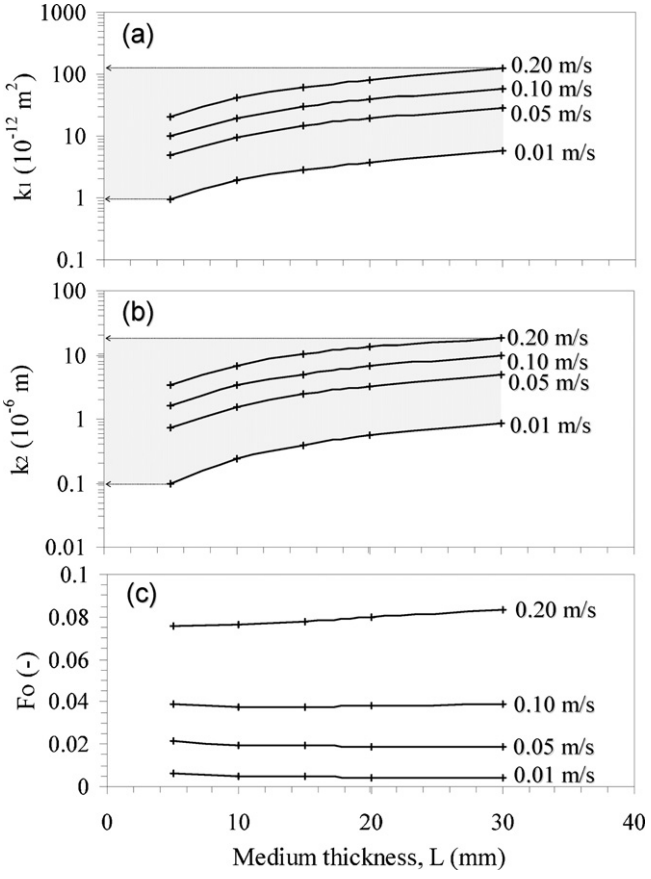

Fig. 1. Required ranges of k_1 (a) and k_2 (b) for ceramic membranes $\Delta P = 1000$ Pa and airflow at ambient conditions; (c) Fo range.

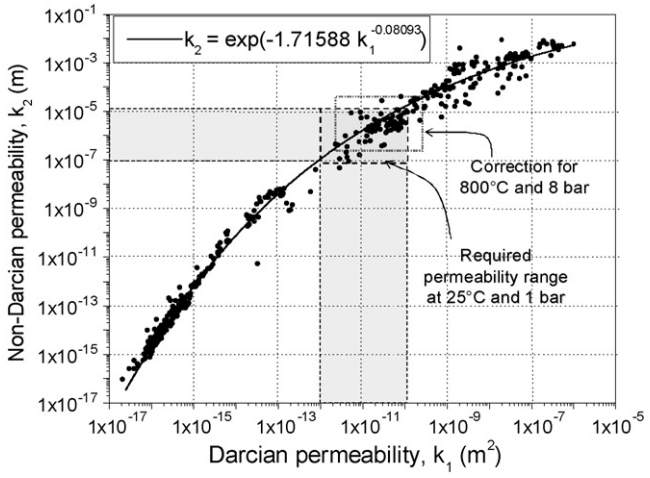

Fig. 2. Required permeability ranges of flat ceramic membranes (30 mm ≥ L ≥ 5 mm) for aerosol filtration.

the former constant is important for permeability characterization (Darcy's law is valid).

For gas flow operation at high temperatures and pressures, fluid properties μ and ρ must be corrected, and so the required values for k_1 and k_2. For instance, for airflow at 800 °C and 8 bar, μ is expected to roughly increase by a factor of 2.5 and ρ by a factor of 2.2, compared to room conditions, so that the curves in Fig. 1 must be recalculated to keep pressure drop unchanged.

Fig. 2 shows an adapted map that links experimental k_1 and k_2 data from different sources in literature [11]. The marked regions locate the permeability range required for ceramic membranes in two flow conditions.

The assessment of the actual values for k_1 and k_2 at the temperature of interest is also very important, since these parameters may be affected by physical changes in the structure during the heat-up (for instance, thermal expansion) [12,20].

The procedure previously described can be repeated for other pressure drop limitations according to the type of application, fluid properties and flow conditions. In general, the increase in the maximum admissible pressure drop for the virgin medium allows the processing of membranes with lower k_1 and k_2 levels or with higher thickness.

1.2. Relationship between permeability and other structural features

Once fixed the permeability needs for the filtration process, the next step is to produce the filtering structure with the desired L, k_1 and k_2 values. Therefore, it is firstly necessary to evaluate how these two latter parameters are qualitatively affected by other measurable physical features of the medium:

Porosity (ε): the increase in the void fraction reduces interstitial velocity and increases the permeability constants. However, only open and interconnected porosity contributes for fluid flow, which is not easily assessed. Simplistic models assume a linear influence of ε on k_1 and a quadratic on k_2 for cellular materials [11]. Typical porosity of commercial hot gas filters is around 40–85%, but it may reach up to 96% for some fibrous elements [4,5,11,18].

Pore size (d_{pore}): the size of particles that can be collected by the filtration media is determined by the size of pores at their most constricted parts. Optimum filtration occurs with dust deposition on the medium surface, after the formation of a uniform cake. The increase of pore size facilitates the penetration of dust

into the porous matrix (deep filtration), with clogging of the filter or reduction of its collection efficiency [12]. In relation to fluid flow, the increase in pore size reduces the friction area, tortuosity, changes in fluid direction and velocity and consequently increases the permeability constants. Some models assume that k_1 and k_2 scale directly with d_{pore}^2 and d_{pore}, respectively, although this trend is still controversial for cellular materials [11]. Typically, pore size of commercial media for hot gas filtration ranges from 0.1 to 10 μm and may reach up to 60 μm for some fibrous media [5,11,18].

The ceramic producer or designer has two options for optimizing the filtering medium permeability based on the processing conditions:

(a) prediction of k_1 and k_2 based on other measurable physical features of the medium that are closely related to processing conditions, such as porosity and pore size;
(b) measurement of k_1 and k_2 and direct association with processing variables based on the ceramic composition, suspension features, polymeric precursor, additives, thermal treatment, etc.

Unfortunately, there has been so far in the literature no agreement about reliable mathematical dependences of k_1 and k_2 with ε and d_{pore}. For this reason, in this work no modelling involving these variables was attempted and permeability constants were directly obtained from experiments.

2. Experimental procedures

Porous ceramic samples were prepared through the incorporation of aqueous foams into alumina-based suspensions [6]. Details of raw materials and proportions for both suspension and foam are given in Table 1.

For preparation of ceramic suspension, powders and part of the liquid were firstly mixed (IKA Mixer, Labortechnik RW 20M) at 500 rpm and then passed with the remaining liquid through a high-energy disperser (IKA, Labortechnik–T25 Basic) at 9500 rpm.

Foam was prepared by mixing all the ingredients (Table 1) at high rotation in a beaker until reach the desired consistency. Ceramic suspension and foam were then mixed together in different volume proportions under gentle mixing to avoid changes in the bubble size distribution. Finally, the setting agent was added under mixing for a few seconds at 800 rpm, followed by moulding. Samples were moulded as disks with diameter of 5 cm and thickness of 7–10 mm. After drying for 24 h at room conditions, samples were heat treated at 1200 °C for 2 h, with a heating rate of 5 °C/min.

Samples were tested for pore size distribution by mercury porosimetry (Micromeritics, model Auto Pore III) and for porosity by water displacement method, based on the Archimedes principle. The splitting tensile strength was obtained for three samples of each batch according to the ASTM C496-90 standard method in a universal testing machine (INSTRON—model 5569) with crosshead velocity of 6 mm/min. Microstructural observation was conducted using scanning electron microscopy (LEO—Model Stereoscan 440) on platinum-coated samples.

Permeability tests were firstly performed with airflow at room conditions ($T \approx 25$ °C, $P_{atm} \approx 715$ mmHg, $\mu \approx 1.86 \times 10^{-5}$ Pa s, $\rho \approx 1.11$ kg/m^3) on 3 bodies of each batch (flow area A of 5.15 cm^2). The experiments evaluated the exit volumetric airflow rate Q through the sample in response to the variations of the inlet pressure P_i applied. Q was measured with soap-bubble flowmeters (0–15 L/min) and rotameters (0–100 L/min) at the exit of the sample and P_i was measured at the inlet chamber with an electronic pressure transducer (0–10 bar).

Permeability constants k_1 and k_2 were obtained by polynomial fitting of Forchheimer's equation to the experimental data according to the least-squares method. Due to the large variation of pressure employed in the tests, Eq. (3) was used to obtain ΔP, with pressure P being set as P_o.

After the analysis of results for the several processed batches, the membranes with better overall performance were chosen for a new set of experiments at high temperature. Permeability tests were then performed isothermally in temperatures ranging from ambient to 700 °C. Atmospheric pressure at the lab location was 691 mmHg and ambient temperature ranged from 16 to 20 °C. The effective flow area through the sample was 7.1 cm^2. The tests consisted in establishing a test superficial air velocity, flowing upwards, and measuring the pressure gradient through the membrane. Pressure P in Eq. (3) was set as P_i, since flow measurements this time were carried out at the inlet air stream ($v_s = v_{si}$). A new filtering membrane was used for each testing temperature. Forchheimer's equation was used to fit permeability constants k_1 and k_2. A schematic view of the permeation rig is shown in Fig. 3, which was also used for the filtration tests.

The collection efficiency tests were carried out at room temperature and also at 700 °C. The test powder utilized was a phosphate rock concentrate (density of 2970 kg/m^3 and average particle size of 4.6 μm). In each test the particles were dispersed in air by a TSI model 3400 fluidized bed aerosol generator and fed into the flowing air stream before the filter entrance. The efficiency was measured by counting the particles before and after the filter with the use of a Hyac-Royco Model 5230 particle counter. For filtration tests, the air velocity was fixed at 0.05 m/s and inlet dust concentration was 17.4 mg/m^3. The number of particles in the air stream was monitored in eight different sizes, 0.75, 1.5, 2.5, 3.5, 4.5, 6.0, 8.5 and 12.5 μm, at the inlet and outlet of the filter.

Introduction of aerosol in the system started 10 min after the preset temperature and air velocity reached the steady state. Filtration time was set at 20 min, whereas the duration of each sampling was 1 min. Particle counting was carried out after 5, 10 and 20 min of operation to verify the effect of the filtration time on the filter performance. The whole procedure was repeated for each testing temperature and sample. The fractionary collection efficiency (η_i) was calculated by converting into mass flow rate the number of particles for each size range i measured at the inlet and outlet of the filter. Total collection efficiency (η_T) of each membrane was obtained by accounting the total mass flow rate of dust entering and leaving the filter.

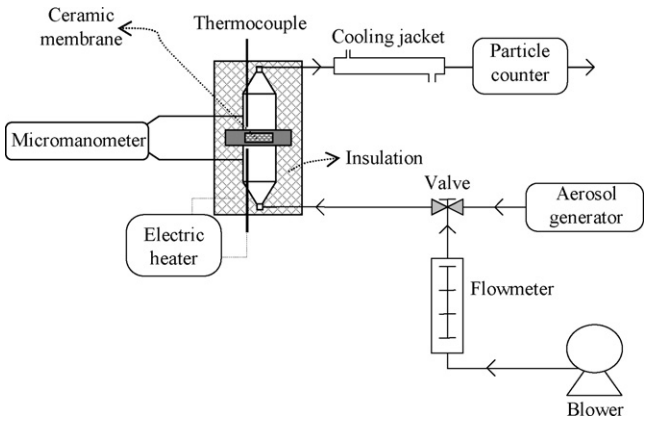

Fig. 3. Schematic apparatus used for permeability and filtration tests.

Table 1
Compositions of porous bodies tested in this work

Raw material	Batch																
	1	2	3	4	5	6	7	8	9	10	11P	12P	12	13	14	1S	2S
Suspension[a]																	
Calcined Alumina A17NE[b]	8.18	8.18	8.18	8.18	7.92	7.92	7.92	7.92	7.92	7.91	7.92	7.92	7.92	7.92	7.92	7.92	7.92
Calcined Alumina CT3000SG[b]	53.19	53.19	53.19	53.19	51.50	51.50	51.50	51.50	51.47	51.44	51.47	51.50	51.50	51.48	51.46	51.48	51.46
Aluminum hydroxide Hydrogard[b]	20.46	20.46	20.46	20.46	19.81	19.81	19.81	19.81	19.80	19.78	19.80	19.81	19.81	19.80	19.79	19.80	19.79
Water	17.36	17.36	17.36	17.36	16.81	16.81	16.81	16.81	16.80	16.79	16.80	16.81	16.81	16.80	16.79	16.80	16.79
Sodium polyacrylate[c]	0.82	0.82	0.82	0.82	0.79	0.79	0.79	0.79	0.79	0.79	0.79	0.79	0.79	0.79	0.79	0.79	0.79
EVA[d]	0.00	0.00	0.00	0.00	3.17	3.17	3.17	3.17	3.17	3.17	3.17	3.17	3.17	3.17	3.17	3.17	3.17
Polypropylene fiber[e]	0.00	0.00	0.00	0.00	0.00	0.00	0.00	0.00	0.06	0.12	0.06	0.00	0.00	0.00	0.00	0.00	0.00
Cellulose fiber[f]	0.00	0.00	0.00	0.00	0.00	0.00	0.00	0.00	0.00	0.00	0.00	0.00	0.00	0.04	0.04	0.04	0.04
PVA[g]	0.00	0.00	0.00	0.00	0.00	0.00	0.00	0.00	0.00	0.00	0.00	0.00	0.00	0.00	0.04	0.00	0.04
Foam[h]																	
Water	47.60	47.60	47.60	47.60	47.60	47.60	47.60	47.60	47.60	47.60	47.60	47.60	47.60	46.67	46.67	46.67	46.67
SLES[f]	4.80	4.80	4.80	4.80	4.80	4.80	4.80	4.80	4.80	4.80	4.80	4.80	4.80	4.71	4.71	4.71	4.71
Glycerine[g]	31.70	31.70	31.70	31.70	31.70	31.70	31.70	31.70	31.70	31.70	31.70	31.70	31.70	31.08	31.08	31.08	31.08
Sodium polyacrylate[c]	15.90	15.90	15.90	15.90	15.90	15.90	15.90	15.90	15.90	15.90	15.90	15.90	15.90	15.59	15.59	15.59	15.59
EVA[d]	0.00	0.00	0.00	0.00	0.00	0.00	0.00	0.00	0.00	0.00	0.00	0.00	0.00	1.96	1.96	1.96	1.96
Setting agent																	
CA14[i]									1.50								
Volume ratio$_{foam}/_{suspension}$	0.0	0.5	1.0	1.5	0.0	0.5	1.0	1.5	1.0	1.0	1.0	1.0	1.0	1.0	1.0	1.0	1.0

[a] Percentages based on total suspension mass.
[b] Alcoa Chemicals, USA.
[c] Clariant Chemicals, Brazil.
[d] Poly(vinyl acetate-co-ethylene), Wacker Chemie AG, Germany.
[e] J. Rettenmaier Latinoamericana Ltda., Brazil.
[f] Votorantim Celulose e Papel, Brazil. Sodium Lauryl Ether Sulphate, Bravir, Brazil.
[g] Poly vinyl alcohol, China National Chemical Fiber Corp. (CNCFC), China. F. Maia Ind. e Com. Ltda, Brazil.
[h] Percentages based on total foam mass.
[i] Calcium Aluminate Cement, Alcoa, USA (percentage based on the mass of suspension).

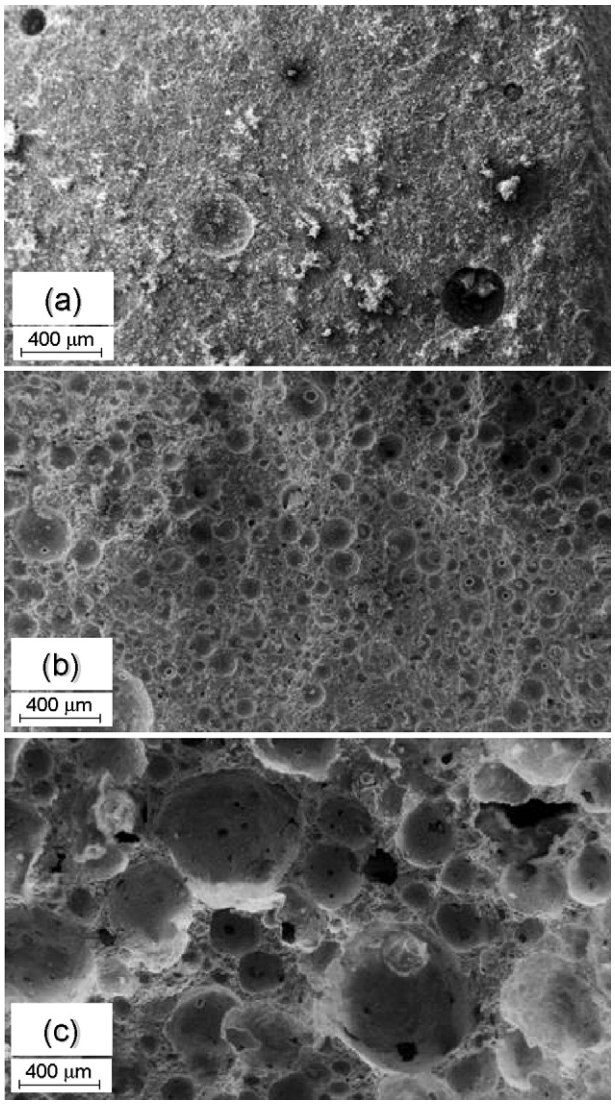

Fig. 4. SEM micrographs of samples: (a) batch 1; (b) batch 3; (c) batch 2S.

3. Results

The incorporation of foam in alumina-based suspension appeared to have caused high level of porosity and narrow pore size distribution. Microstructural examination of filtering membranes produced from alumina suspension with and without incorporation of foam provided direct support to this point as is shown in Fig. 4.

The differences in pore size distribution caused by adjustments in the foam composition or in the foam-to-suspension volumetric ratio are illustrated in Fig. 5. In bodies from batch 1, the paths for fluid percolation in the ceramic matrix were only due to the very small interparticle voids originally filled by the mixing water and later settled by cement hydration. When foam bubbles were incorporated into the matrix, a clear class of larger spherical voids (cells) was created (batch 3). With the increase in the size and amount of foam bubbles, the creation of intersections (windows) among cells resulted in a bimodal pore size distribution (batches 13 and 2S). However, this shift in pore size distribution was not necessarily due to a higher foam volume added to the suspension, but also due to the presence and amount of additives (Table 1).

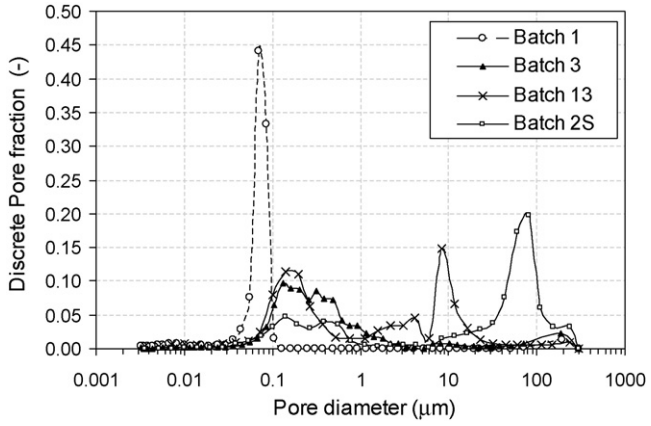

Fig. 5. Typical pore size distributions for some of the tested batches.

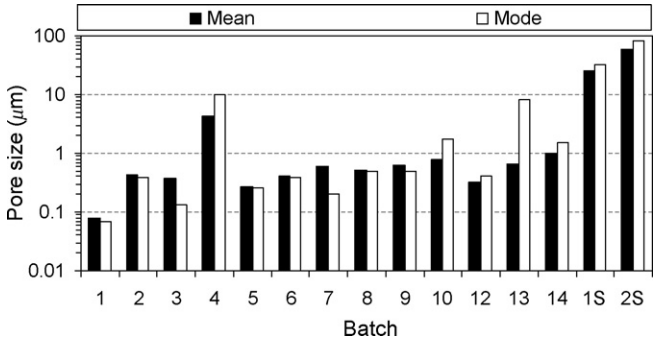

Fig. 6. Average pore sizes of tested batches.

The effects of foam incorporation on the average pore sizes of all batches are better described in Fig. 6. The proximity between mean and mode values is a consequence of the narrow size distributions produced, which is one of the main advantages of this processing method. It is worth noting that although no foam was added in batch 5, the presence of additives (EVA and sodium polyacrylate) caused the incorporation of small air bubbles during the suspension mixing, which explains the higher average pore values compared with batch 1. As expected from mercury porosimetry and observed in Figs. 4–6, the obtained pore distribution was related more to the size of throats (windows) than to the size of cells. The fractions of open and closed pores in each batch are shown in Fig. 6. The true density of the solid material was found to be 3.8 g/cm^3.

Foam addition into the ceramic matrix raised the total porosity level to at least 62%, reaching up to 82% in sample 2S (Fig. 7). Nevertheless, even for samples with a high degree of total

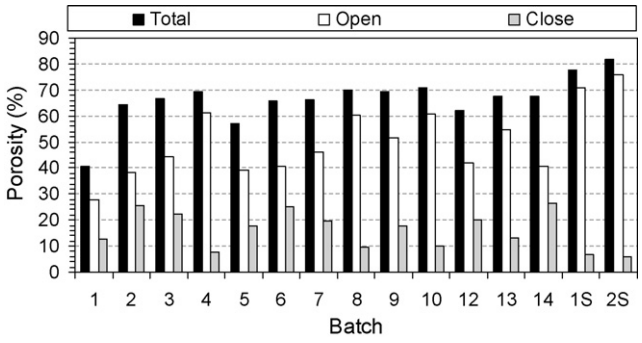

Fig. 7. Porosity levels of tested batches.

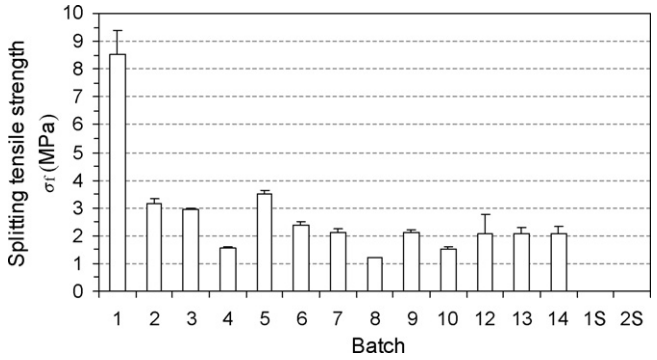

Fig. 8. Splitting tensile strength of tested batches.

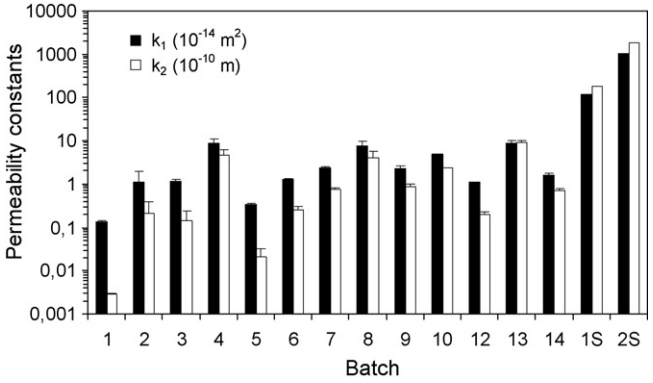

Fig. 10. Permeability parameters k_1 and k_2 of tested batches.

porosity, the closed fraction was large (~25%), as for instance in batches 6 and 14. It means the presence of isolated cells within the ceramic matrix, which do not contribute for fluid flow and only reduces mechanical resistance. For the purpose of the present work, the processing method should provide not only the retention of foam bubbles within the matrix, but also a means to interconnect them. Certain combinations of fibres and additives seemed to work well to produce this effect (Table 1).

The fracture strength σ_f of samples from all batches is shown in Fig. 8. As expected, the higher values were found for samples without foam addition (batches 1 and 5). For other batches, σ_f varied around 1.8–3.2 MPa. No reliable data was available for batches 1S and 2S, because these samples were sliced from a larger cylinder prior to tests.

Typical strength values for commercial ceramic fibre candles are 0.4–1.8 MPa [5,18–19], and for flat foamed ceramics around 3 MPa [6–10]. In the present work, a further improvement could be achieved by the increase in sintering temperature, but probably with reduction of permeability.

Some of the experimental pressure drop curves for evaluation of k_1 and k_2 are shown in Fig. 9. The use of log scales in both axes reflects the great variation in permeability resulted from the processing method. Fig. 10 confirms this trend, where the average k_1 and k_2 values for all batches are presented. The less permeable bodies were those from batches without foam addition (1 and 5), while bodies from batches 1S and 2S (containing PVA and cellulose fibres) were the most permeable ones. A variation over 3 orders of magnitude was found for k_1 and 5 orders for k_2, only by manipulating the foam composition. As expected, there was a direct correspondence of k_1 and k_2 with d_{pore} and with ε and an inverse trend with σ_f.

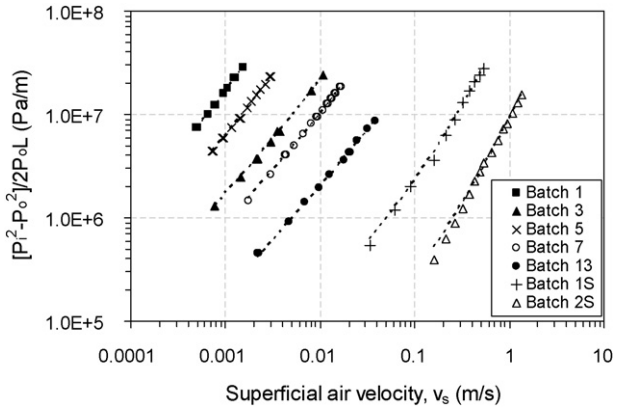

Fig. 9. Typical curves obtained in permeability tests at room temperature. Lines refer to polynomial fitting of Forchheimer's equation.

Fig. 11 shows the resulting range of k_1 and k_2 for the ceramic membranes produced in this work compared to the required ranges for aerosol filtration.

According to Figs. 10 and 11, bodies produced from compositions 4, 8, 13, 1S and 2S were the more promising in terms of a suitable permeability range for aerosol filtration. However, considering other features, such as pore size, porosity level and mechanical strength, compositions 12 and 13 were chosen as the basis for a new set of experiments at high temperatures. For this intent, new bodies were processed following the manufacture procedure previously described. Some minor modifications in the original foam and ceramic compositions were carried out in order to get permeability level further improved.

Physical characterization of membranes 12 and 13 revealed total porosity of 62.1 and 68%, open porosity of 42.1 and 54.8%, mean pore size of 0.33 and 0.67 μm and mode pore size of 0.40 and 8.41 μm, respectively.

Fig. 12 shows typical permeation curves resulting from tests at several temperatures. A decrease in pressure drop is observed with the increase in temperature, which in practice means that less power is required for blowing air at a same flow rate through the membrane.

Fig. 13 shows the influence of temperature on permeability constants for the membranes from batches 12 and 13. The trend of linear increase of k_1 is clear, whereas an irregular trend is observed for k_2. Both parameters are only dependent on structural features

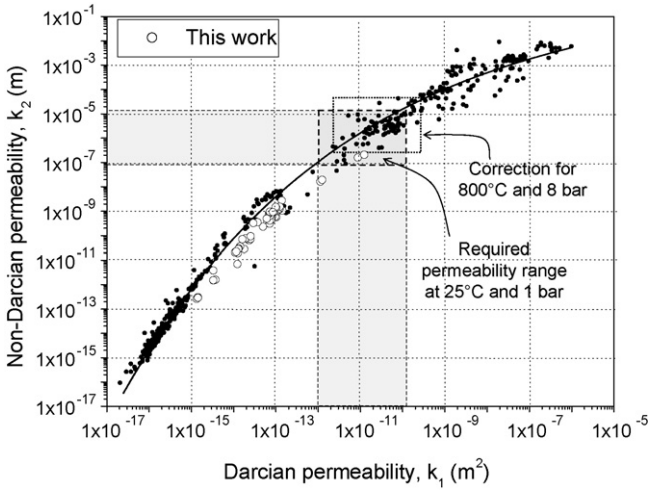

Fig. 11. Comparison of experimental permeability constants of produced membranes and the range required for aerosol filtration.

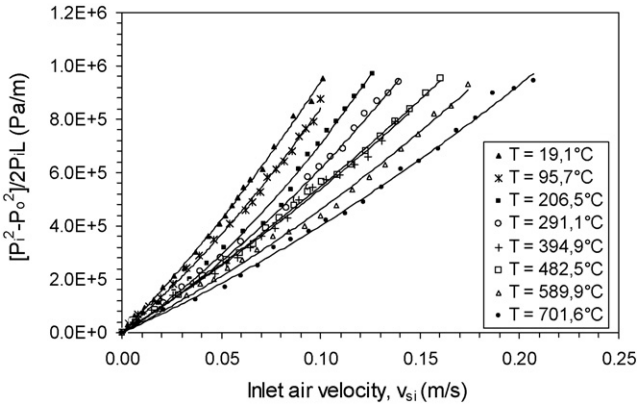

Fig. 12. Typical pressure drop curves obtained from permeation tests at several temperatures with membrane from batch 13. Lines refer to polynomial fitting of Forchheimer's equation.

and consequently changes in their values can be inferred from changes in pore size (d_{pore}), porosity (ε) and pore morphology caused by the temperature increase.

Since samples were previously sintered at 1200 °C for 2 h, no permanent modification was expected to occur in the porous structure during the permeation tests up to 700 °C that would explain changes in k_1 and k_2. In contrast, reversible volumetric variation can take place during the heat-up and the net effect on the flow path depends on the combination of ceramic composition and pore morphology. For instance, the thermal expansion of high-alumina compositions ($\alpha \approx 8 \times 10^{-6}\,K^{-1}$) is higher than that of cordierite ($2MgO.2Al_2O_3.5SiO_2$) compositions ($\alpha \approx 1.8 \times 10^{-6}\,K^{-1}$). However, depending on the pore morphology, such expansion can lead to either a pore constriction or a pore enlargement. The thermal expansion coefficient of cellular materials is essentially the same as that of the solid from which is made [21] and a temporary enlargement in the voids size is then likely to occur with the temperature increase [12]. On the other hand, in high-alumina refractory castables, for which porosity is small and composed by a major fraction of microcrack-like voids at the aggregate–matrix interface, thermal expansion leads to flow path constrictions [12,20].

The literature mentions that k_1 and k_2 scale fairly with d_{pore}^2 and d_{pore} [11], respectively, which implies that the Darcian constant k_1 is more sensitive than the non-Darcian constant k_2 to changes in pore size caused by the temperature increase. This effect seems to explain the more pronounced linear increase for k_1 up to 700 °C as shown in Fig. 13.

It is also worth noting that for the tested superficial velocity range (0–0.2 m/s), the mean Reynolds number at the pore level, Re_{pore}, calculated with the pore size and porosity measured at ambient conditions and density and viscosity of the air corrected for each testing temperature, was always lower than 0.01 in the range 20–700 °C, which indicates a laminar regime with a minor influence of inertial effects. This fact could have precluded a reliable quantification of the quadratic term in Forchheimer's equation and consequently of k_2 values, which would explain the irregular trend observed for this parameter in Fig. 13 with the temperature increase. As a whole, results indicate that for typical gas filtration velocities ($v_s < 0.10$ m/s), Darcy's law is suitable for predicting the pressure drop through membranes 12 and 13, when only the linear term of Eq. (1) becomes important.

Fig. 14 shows the fractionary efficiency results obtained for filtration tests conducted at 20 °C and at 700 °C. Virgin membranes were used in each test, and the initial pressure drop for operation at a face velocity of 0.05 m/s varied from 200 to 450 mmH_2O (2000 and 4500 Pa).

In general, both membranes had similar behaviour. As expected, collection efficiency was higher for larger dust particles, reaching 99.9% for $d_p > 8$ μm, but a poor efficiency for particles below 2 μm was clear for tests at 700 °C. Part of this adverse effect can be explained by the increase in size and volume of the void fraction by thermal expansion, as previously discussed. But, changes in the gas and particle properties may also play a role in filtration behaviour.

In fact, the collection efficiency in a barrier filter is a sum of contributions of several mechanisms. At the initial stages of filtration, the contact between the collector and airborne particles promotes the dust capture based on diffusional, inertial impaction, direct interception, gravitational and electrophoretic mechanisms. As the dust is retained on the filter surface, the built cake acts itself as the main barrier and dust collection is largely enhanced [12].

Theoretically, for a medium with no influence of thermal expansion, the increase in temperature should slightly enhance collection by the diffusional and gravitational mechanisms, but also should cause a reduction in efficiency by the inertial mechanism [12,19].

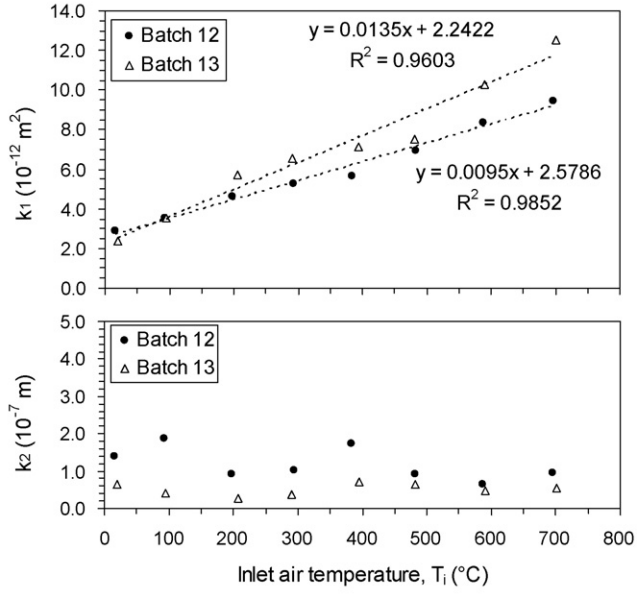

Fig. 13. Influence of temperature on the permeability parameters k_1 and k_2 of membranes.

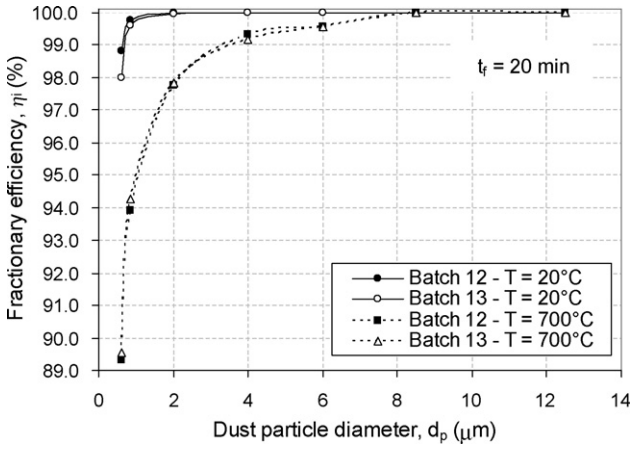

Fig. 14. Fractionary efficiency for membranes 12 and 13 at room temperature and 700 °C.

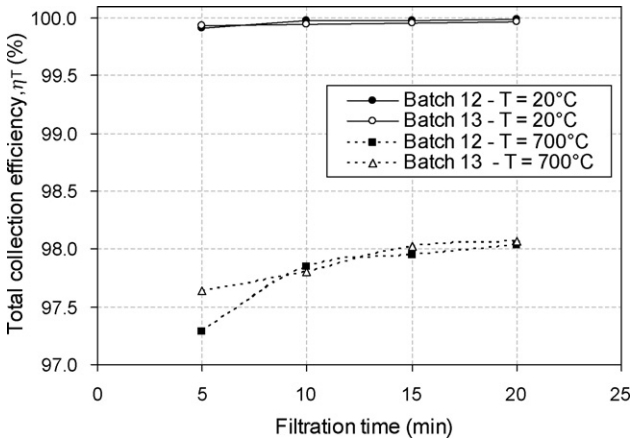

Fig. 15. Total efficiency for membranes 12 and 13 at room temperature and 700 °C as a function of time.

The net effect on dust-removing will depend on the dominant mechanism and therefore on the size of dust particles. In the present work, such analysis is more complex, because thermal expansion affected the structure and efficiency measurements started after 5 min, when the process could probably be no longer time-independent (due to the build up of a small dust cake on the filter surface). For instance, the increase in porosity due to thermal expansion could cause a deleterious effect more important on the diffusional mechanism than the helpful increase in the diffusivity coefficient, which would explain the small collection for particles below 2 μm at 700 °C. Nevertheless, a previous work with alumina filters has demonstrated the theoretical and experimental decrease of efficiency for increasing temperatures up to 700 °C, using the same testing powder and similar operational conditions [12].

Fig. 15 shows that an improvement in total collection efficiency is obtained along the filtration time. The effect was more pronounced for tests at 700 °C, for which efficiency was lower. For tests at room temperature, practically no effect of time was observed, as efficiency approached 99.9% already at the beginning of the test.

Atmospheric emissions of particulate matter (PTS) from boilers based on combustion of sugarcane bagasse are typically in the order of 29 $g_{dust}/kg_{dry\,air}$ or 3500–6000 mg/m^3 [1,2]. On the other hand, the Brazilian Resolution no. 382, from the National Environmental Council (CONAMA) stipulates an emission limit from 200 to 280 mg/m^3 (expressed in dry basis with 8% oxygen excess) [3]. In practice it implies that the gas cleaning technology for this particular application must have an overall particle collection efficiency of at least 97% to meet environmental regulation. Nowadays, spray tower and venture-type scrubbers have attended this requirement in Brazilian industry, but with loss of thermal energy in the gas stream, high consumption of water and also generation of a slurry effluent that must be treated. In this sense, membranes obtained from both compositions 12 and 13 seem to be promising to meet the efficiency requirement of a dry collection technology. However, further tests are required to confirm the collection efficiency and pressure drop performances along several filtration cycles.

4. Conclusions

(a) In this work, ceramic membranes were processed according to the technique of incorporation of aqueous foams into alumina-based suspensions. Among the tested compositions, it was possible to choose those with suitable permeability range to be used in aerosol filtration applications.

(b) The selected compositions had their permeability evaluated in tests under temperatures up to 700 °C. Results revealed that the Darcian permeability constant k_1 increases with temperature and that Darcy's law is suitable to represent the pressure drop across the membranes. The net effect of temperature was a favourable decrease in pressure drop.

(c) Filtration tests at room temperature confirmed that both chosen compositions had collection efficiencies high enough to meet emission limits established by Brazilian regulations.

(d) Filtration tests at 700 °C revealed a significant reduction in fractionary and total collection efficiency. Part of this behaviour was related to reversible thermal expansion effects during the heat-up and part to the changes in fluid properties, which changed collection according to the several mechanisms that act in a barrier filter. Improvements in the ceramic composition to minimize these effects are in progress.

Acknowledgements

Authors gratefully acknowledge the support given by FAPESP, CAPES and MCT/CNPq Process CT-Energ 551601/2005-1.

References

[1] E.E.S. Lora, Controlling Air Quality in the Cane Sugar Industry, vol. 1, first ed., Bartens, Berlin, Germany, 2001, p. 202.
[2] EPA, Compilation of Air pollutant Emission Factors, vol. 1, fifth ed., Stationary Point and Area Sources, U.S. Environmental Protection Agency, AP-42, 1995.
[3] CONAMA, National Environmental Council, Resolution no. 382/2006, Brazilian Environment Ministry, Brasília - Brazil, 2006 (in Portuguese).
[4] D. Fino, G. Saracco, Gas (particulate) filtration, in: M. Scheffler, P. Colombo (Eds.), Cellular Ceramics: Structure, Manufacturing, Properties and Applications, 2005, pp. 416–438.
[5] J.P.K. Seville, R. Clift, C.J. Withers, W. Keidel, Rigid ceramic media for filtering hot gases, Filtration and Separation (July/August) (1989) 265.
[6] R.C.O. Romano, V.C. Pandolfelli, Production and properties of porous ceramics obtained by foam addition technique, Cerâmica 52 (2006) 213–219 (in Portuguese).
[7] L. Biasetto, P. Colombo, M.D.M. Innocentini, S. Mullens, Gas permeability of microcellular ceramic foams, Industrial & Engineering Chemistry Research 46 (2007) 3366–3372.
[8] M.D.M. Innocentini, P. Sepulveda, V.R. Salvini, J.R. Coury, V.C. Pandolfelli, Permeability and structure of cellular ceramics: a comparison between two preparation techniques, Journal of the American Ceramic Society 81 (12) (1998) 3349–3352.
[9] P. Sepulveda, F. Ortega, M.D.M. Innocentini, V.C. Pandolfelli, Properties of highly porous hydroxyapatite obtained by the gelcasting of foams, Journal of the American Ceramic Society 83 (12) (2001) 3021–3024.
[10] F. Ortega, P. Sepulveda, M.D.M. Innocentini, V.C. Pandolfelli, Surfactants: a necessity for producing porous ceramics, American Ceramic Society Bulletin 80 (4) (2001) 37–42.
[11] M.D.M. Innocentini, P. Sepulveda, F. Ortega, Permeability, in: M. Scheffler, P. Colombo (Eds.), Cellular Ceramics: Structure, Manufacturing, Properties and Applications, 2005, pp. 313–340.
[12] N.L. Freitas, J.A.S. Gonçalves, M.D.M. Innocentini, J.R. Coury, Development of a double-layered ceramic filter for aerosol filtration at high-temperatures: the filter collection efficiency, Journal of Hazardous Materials B136 (2006) 747–756.
[13] M.D.M. Innocentini, A.R.F. Pardo, V.R. Salvini, V.C. Pandolfelli, Assessment of Forchheimer's equation to predict the permeability of ceramic foams, Journal of the American Ceramic Society 82 (7) (1999) 1945–1948.
[14] M.D.M. Innocentini, W.L. Antunes, J.B. Baumgartner, J.P.K. Seville, J.R. Coury, Permeability of ceramic foams to gas flow, Advanced Powder Technology 299 (1999) 19–28.
[15] M.D.M. Innocentini, V.R. Salvini, A. Macedo, V.C. Pandolfelli, Prediction of ceramic foams permeability using Ergun's equation, Materials Research 2 (4) (1999) 283–289.
[16] M.D.M. Innocentini, V.R. Salvini, J.R. Coury, V.C. Pandolfelli, The permeability of ceramic foams, American Ceramic Society Bulletin 78 (9) (1999) 78–84.
[17] D. Hlushkou, U. Tallarek, Transition from creeping via viscous-inertial to turbulent flow in fixed beds, Journal of Chromatography A 1126 (2006) 70–85.

[18] R.K. Ahluwalia, V.J. Novick, L. Zhang, M.P. Sutaria, J.P. Singh, Performance of a vacuum formed chopped ceramic fiber filter in a reducing environment, Journal of Engineering for Gas Turbines and Power 123 (April (2)) (2001) 293–302.
[19] W. Cheung, Filtration and cleaning characteristics of ceramic media, Ph.D. Thesis, University of Surrey, UK, 1989.
[20] M.D.M. Innocentini, M.G. Silva, B.A. Menegazzo, V.C. Pandolfelli, Permeability of refractory castables at high-temperatures, Journal of the American Ceramic Society 84 (3) (2001) 645–647.
[21] M.F. Ashby, Cellular solids—scaling of properties, in: M. Scheffler, P. Colombo (Eds.), Cellular Ceramics: Structure, Manufacturing, Properties and Applications, 2005, pp. 3–16.